ACADEMIC PRESS

Available online at www.sciencedirect.com

SCIENCE DIRECT®

Experimental Cell Research 289 (2003) 58–66

Experimental Cell Research

www.elsevier.com/locate/yexcr

Measuring the mechanical stress induced by an expanding multicellular tumor system: a case study

V.D. Gordon,[a,b] M.T. Valentine,[a,b] M.L. Gardel,[a,b] D. Andor-Ardó,[a] S. Dennison,[b] A.A. Bogdanov,[c] D.A. Weitz,[a,b,*] and T.S. Deisboeck[a,d,e]

[a] *Division of Engineering and Applied Sciences, Harvard University, Cambridge, MA 02138, USA,*
[b] *Department of Physics, Harvard University, Cambridge, MA 02138, USA*
[c] *Center for Molecular Imaging Research, Massachusetts General Hospital, Harvard Medical School, Charlestown, MA 02129, USA*
[d] *Complex Biosystems Modeling Laboratory, Harvard-MIT (HST) Athinoula A. Martinos Center for Biomedical Imaging, HST-Biomedical Engineering Center, Massachusetts Institute of Technology, Cambridge, MA 02139, USA*
[e] *Molecular Neuro-Oncology Laboratory, Massachusetts General Hospital, Harvard Medical School, Charlestown, MA 02129, USA*

Received 26 November 2002, revised version received 11 April 2003

Abstract

Rapid volumetric growth and extensive invasion into brain parenchyma are hallmarks of malignant neuroepithelial tumors in vivo. Little is known, however, about the mechanical impact of the growing brain tumor on its microenvironment. To better understand the environmental mechanical response, we used multiparticle tracking methods to probe the environment of a dynamically expanding, multicellular brain tumor spheroid that grew for 6 days in a three-dimensional Matrigel-based in vitro assay containing 1.0-μm latex beads. These beads act as reference markers for the gel, allowing us to image the spatial displacement of the tumor environment using high-resolution time-lapse video microscopy. The results show that the volumetrically expanding tumor spheroid pushes the gel outward and that this tumor-generated pressure propagates to a distance greater than the initial radius of the tumor spheroid. Intriguingly, beads near the tips of invasive cells are displaced inward, toward the advancing invasive cells. Furthermore, this localized cell traction correlates with a marked increase in total invasion area over the observation period. This case study presents evidence that an expanding microscopic tumor system exerts both significant mechanical pressure *and* significant traction on its microenvironment.

Keywords: Brain tumor; Multicellular tumor spheroid; Growth dynamics; Invasion; Traction; Stress; Strain; Matrigel; In vitro assay; Particle tracking; Microrheology

Introduction

The outcome for patients suffering from highly malignant brain tumors remains dismal despite all therapeutic efforts. The most malignant form, glioblastoma, which accounts for 23% of all primary brain tumor cases, has a mean patient age at diagnosis of 65 years and, in the age group of 45 and older, a 5-year relative survival rate of below 2.1% [1]. The reasons for the almost inevitable treatment failure include rapid volumetric growth, early development of treatment resistance, and, most importantly, extensive tissue infiltration, which leaves these neoplasms surgically incurable.

A better understanding of the structural remodeling of brain parenchyma by tumor proliferation and invasion is essential to understanding the processes that facilitate diffuse infiltration and tumor recurrence. However, the mechanical relationship between an expanding tumor system and its microenvironment is still poorly understood. By placing multicellular tumor spheroids in increasing concentrations of an agarose gel, Helmlinger et al. [2] found that such spheroids can overcome a mechanical stress of up to 45 mmHg (6 kPa) before they become growth-inhibited at stresses between 45 and 120 mmHg (6 and 16 kPa). Fur-

* Corresponding author. Department of Physics, Harvard University, Cambridge, MA 02138. Fax: +1-617-496-9564.
E-mail address: weitz@deas.harvard.edu (D.A. Weitz).

0014-4827/03/$ – see front matter © 2003 Elsevier Science (USA). All rights reserved.
doi:10.1016/S0014-4827(03)00256-8

thermore, in addition to withstanding pressure, neoplastic cells much like normal cells may also exert traction. The traction forces generated by skin fibroblasts have been measured by Delvoye et al. [3] via strain-gauge measurements. Using distortable sheets of silicone rubber, Harris et al. [4] established a method by which traction forces exerted by individual cells can be visualized. In fact, they distinguish "compression wrinkles," directly beneath the traction-generating cell, from "tension wrinkles," which radiate outward. Interestingly, in their follow-up article [5] the authors compare various cell types and observe that glia cells from dorsal root ganglia exert very strong traction forces. Since then, a variety of methods and several other gels, including polyacrylamide gels, collagen gels, and basement membrane gels, have been used to study mechanical stresses at the cell–substrate interface [e.g., 6,7]. For instance, reorganization of basement membrane matrices has been studied extensively with endothelial cells and fibroblasts. Using Matrigel, a commercial basement membrane gel, Vernon et al. [8] reported that cellular traction leads to extracellular matrix (ECM) alignment, in which matrix filaments form lines or tracks; this alignment promotes cellular elongation and directs migration. This leads ultimately to the formation of multicellular cords and tubelike structures, characteristic of endothelial cells. Moreover, a quantitative correlation of "contact guidance" with collagen fibril orientation has been described for human fibroblasts [9]. These traction forces can have significance for remodeling connective tissue by tumors as well. In fact, contraction of collagen fibrils has been linked to the metastatic potential of melanoma cells [10] and may also be important for cell locomotion in other cancers, including malignant brain tumors.

Tumor tissue invasion itself is a multistep process, however, including cell attachment, degradation of ECM components, and active cell motility. ECM degradation in turn requires the expression of proteolytic enzymes by the tumor cells, which has been shown to occur in gliomas in vitro and in vivo [11,12]. Interestingly, the parental (high-grade glioma) cell line of the one used in our experiment, U87MG, has been shown to release gelatinase A, known also as metalloproteinase 2 (MMP-2) [12,13]. As Chintala et al. [14] have reported, MMP-2 can degrade a variety of ECM components, including collagen IV, which is a major (30%) ECM component of the bio-gel used in our assay. A rather complex interplay between mechanical forces and proteolytic enzymes is supported by the work of Vernon and Sage [15], who studied the remodeling of collagen type I gels by bovine aortic endothelial (BAE) cells. Using zymography to detect enzymatic activity, the authors found that BAE cells that had contracted collagen gels also had secreted MMP-2. They conclude that both cellular traction and proteolysis are important for endothelial cell invasion in the process of angiogenesis.

To elucidate the role of and potential interplay between compression and traction in the dynamic expansion of a microtumor system, we implanted a growing multicellular (brain) tumor spheroid (MTS) in a gel matrix and investigated the tumor's impact on its ECM gel microenvironment with methods from microrheology. Specifically, we used 1.0-μm beads as reference markers for the gel and monitored their spatial displacement with high-resolution time-lapse video microscopy. In addition, videorate imaging and particle tracking were employed to study the thermally driven Brownian motions of these tracer beads. In the vicinity of invasive tips, such position fluctuations remain constant in size throughout the observation period. The results show not only that the volumetrically expanding spheroid *pushes* the gel outward but also that beads near the tips of advancing invasive cells are displaced inward, toward these tips. This is consistent with cell *traction* producing tension in the gel. In addition, significant localized gel strain toward invasive cell tips correlates well with a marked increase in overall gel invasion throughout the observation period, indicating that cell traction and invasion are linked. To our knowledge this is the first study presenting evidence that a growing microscopic tumor system can exert *both* significant pressure and traction on its microenvironment.

Materials and methods

Multicellular tumor spheroid and morphometric measurements

The human U87MGmEGFR glioblastoma cell line[1] was used to generate the multicellular tumor spheroids (MTS) [16]. We cultured this cell line in DMEM medium (Gibco BRL, Life Technologies, Grand Island, NY) supplemented with 10% heat-inactivated cosmic bovine serum (HyClone, Logan, UT) and 400 μg/ml G418 (Life Technologies) in a humidified atmosphere (at 37°C and 5% CO_2). These cells coexpress both wild-type epidermal growth factor receptor and its mutant variant, mEGF-R [17]. U87MGmEGFR cells tend to form spheroids in culture after reaching monolayer confluence. Once detached, these spheroids can be collected from the medium with Pasteur pipettes. A variation of the assay used here is described in Deisboeck et al. [18].

In the present case study, we used a rather small spheroid, less than 200 μm in diameter, that we placed in a novel $1 \times 1 \times 1$ cm plexiglass cube filled with a 3:1 mixture of growth factor reduced (GFR) matrix, Matrigel (BIOCAT, Becton–Dickinson, Franklin Lakes, NJ), and (non-serum supplemented) OPTI-MEM medium at 4°C, at which temperature the mixture remains fluid. The spheroid settled to lie close to the bottom of the cube and several hundred microns from vertical walls (while the gel mixture was still fluid), and it remained at this location after the medium

[1] Kindly provided by Dr. W.K. Cavenee (Ludwig Institute for Cancer Research, San Diego, CA).

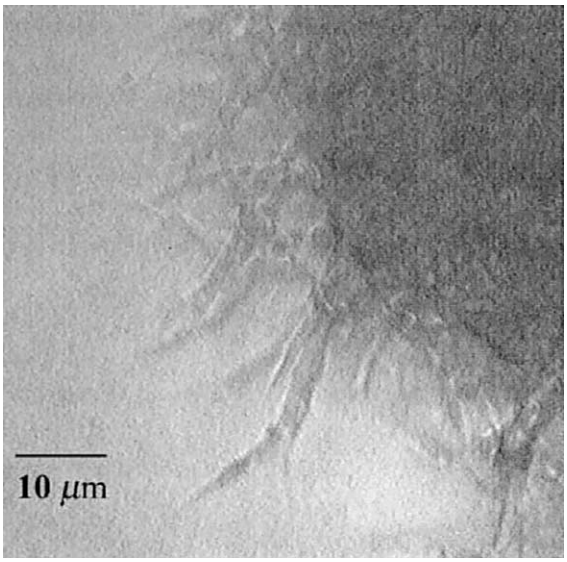

Fig. 1. Multicellular tumor spheroid (MTS) with invasive branches. Taken on Day 3, the image displays a part of the main tumor (dark gray) and shows invasive branches originating from the surface of the MTS. Forming these branches, invasive cells advance in a chainlike pattern (original magnification: ×10).

gelled. When raised to room temperature, this mixture gels to form a reconstituted basement membrane. Because the liquid matrix gelled in situ about the spheroid, there should be no stress in the matrix associated with the introduction of the spheroid. Latex beads, 1 μm in diameter, were dispersed in this assay mixture at 4°C while it was still liquid, before the tumor spheroid was inoculated, so that they are incorporated into the gel matrix surrounding the MTS. Maintaining the assay at 37°C and 5% CO_2, tumor growth and invasion as well as the bead-containing microenvironment were imaged at both time lapse (1 frame per 30 s) and video rates (30 frames per second), allowing particle tracking and analysis of bead motions. The gelled sample, including tumor spheroid and beads, remained in the plexiglass cube for the 6-day observation period. Figure 1 shows part of the tumor approximately 48 h after implantation. The dark-gray area is part of the central MTS; lighter invasive branches, consisting of mobile tumor cells following each other in chainlike migration, are also depicted.

The maximum orthogonal diameters of the MTS were measured at an original magnification of ×10 and the average diameter, D_{MTS}, determined with an uncertainty of less than 5 μm, was used to calculate the volume, V_{MTS} of the MTS core as follows:

$$V_{MTS} = \frac{\pi D_{MTS}^3}{6}. \quad (1)$$

The average diameter of the entire tumor system, D_{SYS}, which includes the proliferative MTS core and invasive branches, was determined from measurements of orthogonal diameters of the tips of the invasive chains with an uncertainty of less than 10 μm. From this, the cross-sectional area, A_{SYS}, was calculated using the following:

$$A_{SYS} = \pi\left(\frac{D_{SYS}}{2}\right)^2. \quad (2)$$

The annular cross-sectional area of the invasive region only, A_{INV}, excluding the MTS cross-sectional area, A_{MTS}, can then be calculated with the following:

$$A_{INV} = A_{SYS} - A_{MTS}. \quad (3)$$

Multiparticle tracking

Particle tracking techniques, already well-developed for studying soft materials, have the advantage in the present case of allowing nondestructive in situ measurements over several days to examine the effects of a growing, invading tumor on its local and extended environments. To act as reference markers, latex beads, 1 μm in diameter, were mixed with the liquid Matrigel solution at 4°C so that the beads were evenly dispersed before the tumor spheroid was added and gelation induced.

Carboxylated beads were purchased from Interfacial Dynamics Corporation (Portland, OR) and their surfaces coated with amine-terminated PEG chains (MW = 750 Da) that were covalently coupled to the surface carboxyl groups. The empirical observation that PEG-coated materials resist nonspecific protein adsorption has led to the widespread use of PEG in biomedical applications [19], and we have observed that beads coated with PEG using this protocol are much more resistant than untreated beads to protein adsorption [20]. PEG coating was found to prevent the beads from aggregating together in the gel, allowing more even dispersion and better tracking accuracy. Resistance to protein adsorption also allows the beads to diffuse thermally within the confines imposed by the Matrigel microenvironments.

During tumor growth, the strain field induced in the gel matrix was mapped, via these probe beads, using time-lapsed images acquired using a Hamamatsu CCD camera controlled by Metamorph imaging software (Universal Imaging Corporation, Downingtown, PA). In-house IDL particle-tracking routines [21] were used to analyze the images and Adobe Photoshop 6.0 was used for further image processing. In Figs. 4–7, the color superimposed at a position along a bead track indicates the time elapsed from the beginning of the time-lapse sequence until the bead was at that position: For each time-lapse sequence, each frame has been assigned an unique color value based on its order within the sequence, starting at indigo blue for early times and shading along the spectrum to red at late times. The increment in color value per frame is adjusted according to the number of frames in the sequence, so that the scaling of color with elapsed time is different for each time-lapse sequence.

Furthermore, videorate images of the same field of view were taken using a Sony SVO-9500MD videocassette re-

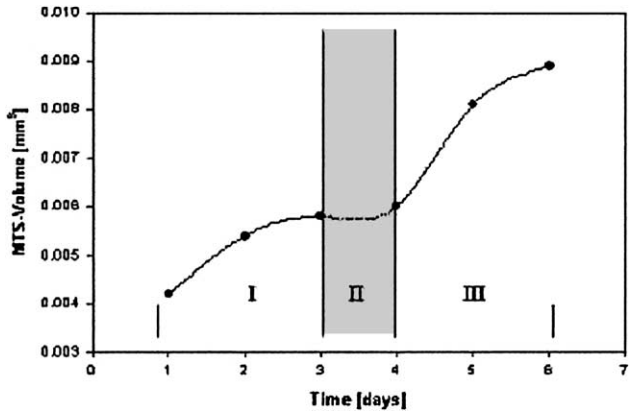

Fig. 2. MTS volume. Volume of the tumor spheroid over 6 days of observation is shown. The gray shading and roman numerals indicate the three growth phases described in the text.

corder immediately before beginning and immediately after completing most time-lapse sequences; this allowed analysis of the beads' thermal motions. We were able, over the course of the study, to examine Brownian bead position fluctuations near and far from the growing tumor and at the tips of invasive branches. The Brownian position fluctuations of embedded beads have been used to study the microrheology [22] as well as the local microenvironments [23] of inhomogeneous soft materials.

We measured the bulk elastic modulus, G', of the Matrigel-based assay, using a temperature-controlled strain-controlled rheometer (C-VOR rheometer, Bohlin Instruments, East Brunswick, NJ) to be 20–40 Pa for frequencies from 0.05 to 100 rad/s. The viscous modulus was an order of magnitude smaller than the elastic modulus for most of the frequency range examined, indicating that the gel is predominantly a *solid.*

Results

Morphometric measurements

Over the 6-day observation period the MTS volume grows from 0.004 to 0.009 mm^3 (Fig. 2) in three phases: initial growth, phase I (Days 1–3); plateaued volume, phase II (Days 3–4); and rapid secondary growth, phase III (Days 4–6). The invasion cross-sectional area increases from 0 to 0.10 mm^2 (Fig. 3) over these 6 days, showing its most rapid expansion between Days 3 and 4. This marked increase in invasion area precedes the secondary volumetric growth (III); similarly, the invasion area plateau (Days 2–3) precedes the MTS volume plateau (II).

Timelapse multiparticle tracking

As the tumor system grows volumetrically and invades the surrounding gel matrix, time-lapse image sequences show the displacements of beads, embedded in the gel, following local gel motion. These reference markers allow the gel's time-dependent strain field induced by the tumor to be mapped, at a variety of locations, over the period of observation.

Four hours after implantation (Day 1), bead tracks in Fig. 4 depict gel movement radially inward toward the tumor. Tracks show movement with a circumferential component, along a line tangential to the tumor surface, as well as a radial component (upper center of image) at a location where an early invasive cell is later seen to emerge. Significant tumor growth begins about 6 h after implantation. The increase in MTS volume (see Fig. 2) displaces the gel radially outward (Fig. 5). Tracks show more circumferential movement (middle right of image) at a location where a cluster of invasion pathways has appeared by the end of this 21-h timelapse sequence. Twenty-four hours after implantation, MTS growth continues to displace gel radially outward (Fig. 6). However, an emergent invasion pathway (center of image) is associated with a local gel strain with a significant component radially inward, toward the tip of the invading cell and opposite to the bulk gel movement. In Fig. 7, 3 days after implantation of the MTS (Day 4) and approximately 65 μm from the spheroid edge, gel near the tip of an invasive branch moves a significant distance in toward the leading invasive cell. Meanwhile, the bulk surrounding gel is only slightly displaced outward. The magnitude and spatial extent of inward strain associated with the invasion is highly directional and not isotropic about the cell tip. The movements of beads more than 30 μm from the leading tip of the invasive cell indicate that the gel here is significantly strained in toward the tip. Gel strain inward toward invasive cell tips is consistently observed throughout this study. Established invasion pathways close to the MTS seem to induce gel strain outward, along the direction of invasion.

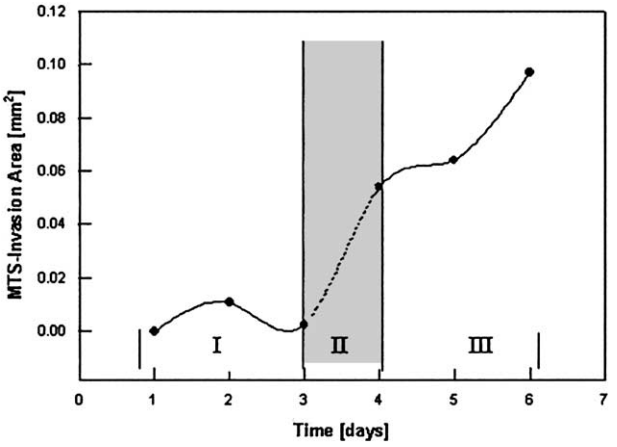

Fig. 3. MTS invasion area. Total invasion cross-sectional area, exclusive of the central MTS core, over the 6 days of observation is shown.

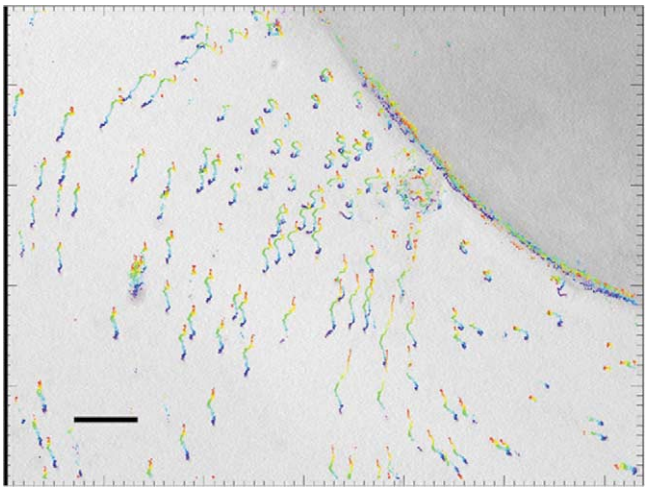

Fig. 4. Time-lapse multiparticle tracking (Day 1). Tracks are drawn to trace the paths of moving beads as color is used to time stamp bead positions: early times are indigo blue and colors shade along the spectrum to red at late times. The tracks have been superimposed on the first frame in the time-lapse sequence. Note darkened multicellular tumor spheroid (top right). Ticks indicate acquired image dimensions, 10 pixels per tick mark (bar = 10 μm; original magnification: ×40; time-lapse duration: 110 min).

Mean square displacement of beads

Throughout the period of observation, the bead-averaged mean square displacement (MSD) for groups of Brownian beads near invasive tips, at a lag time of 0.3 s averaged over 3 to 6 min, remained within the range of 0.012–0.022 μm^2, showing displacements much less than the 1-μm bead diameter.

Observed MSD plateau values were at least 10^2 times larger than those that should be shown for 1-μm Brownian beads probing a continuum medium with an elastic modulus of 30 Pa, our gel's modulus as measured by bulk rheology. Such large MSDs are observed for 1-μm beads in tumor-free as well as tumor-bearing gel matrices. Furthermore, beads with diameters 0.1, 0.2, 0.5, and 1 μm, in tumor-free assays, show plateaued MSD values independent of bead size; bead motions constrained by an elastic modulus should have saturated MSD values depending inversely on bead size. This suggests that the particles are not probing the gel's elastic modulus but rather the microvolume defined by constraining gel fibers.

Discussion

The combination of this 3D ECM gel assay with analytical methods from microrheology and soft condensed matter science yields novel and important insights into the dynamic interaction between tumor and microenvironment. The time-lapsed imaging of tracer beads embedded in the gel matrix allows direct mapping of the displacement field induced by the tumor within its microenvironment and clearly shows that the volumetrically expanding tumor spheroid displaces the bulk matrix radially outward, whereas gel near the tips of invasive cells is pulled inward toward those tips. Since such gel reportedly consists of interconnected sheets of proteins [24], these phenomena should be attributed to *stress propagation*, that is, movement of distant beads results from transmission of the local mechanical effect exerted by the expanding tumor or by the tip of an invasive branch. In the following, we discuss observations of the microtumor system expanding within the 3D environment, on both *single-cell* and *multicellular* scales, as well as implications of the material properties found in our investigation of the tumor-free Matrigel-based gel mixture.

Qualitative observations of gel displacement and cell traction are not all that can be obtained from these time-lapse sequences. Equipped with knowledge of the gel's bulk viscoelastic properties, we can *quantitatively* estimate the traction exerted by invasive cells. Figure 7, depicting the result of a time-lapse sequence acquired for 165 min during a period of rapid invasion and negligible volumetric growth, shows that beads 7–14 μm from the leading invasive cell tip (tracks 2 and 3) are displaced about 8 μm in toward the tip. One bead about 30 μm from the tip (track 1) is displaced about 5 μm. Gel 46 μm from the cell tip is effectively motionless, probably as a result of the superposition of the invasive tip's inward pull and the growing spheroid's outward displacement, as shown in Fig. 7 by the beads most distant from the invasive cell. We therefore treat the matrix at a distance of 46 μm from the cell tip as fixed and can approximate the unstrained length of gel at a distance r from the cell tip as $L = 46\ \mu m - r$. From this, we find the strain $\Delta L/L$ induced in the gel by the cell tip is approximately 8 μm/(46 μm −14 μm) ≈ 5 μm/(46 μm −30 μm) ≈ 0.3. This indicates that the gel is behaving approximately as a

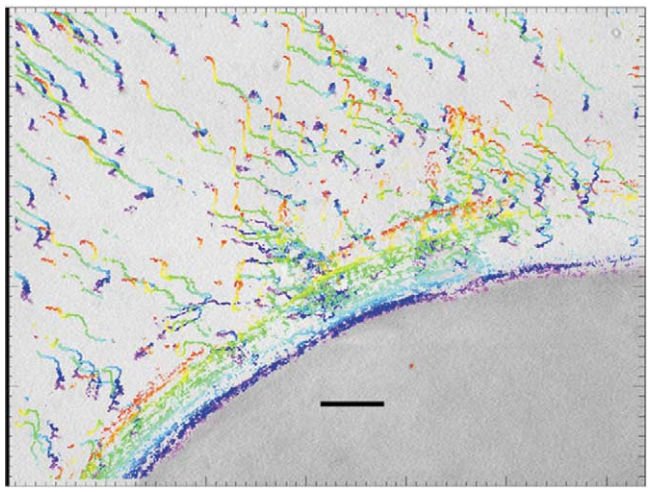

Fig. 5. Time-lapse multiparticle tracking (Day 1). For orientation, note darkened MTS (bottom right). The MTS radius, determined from the colored arcs tracing the outgrowing spheroid edge, increased by more than 10 μm while this sequence was acquired (bar = 10 μm; original magnification: ×40; time-lapse duration: 832 min).

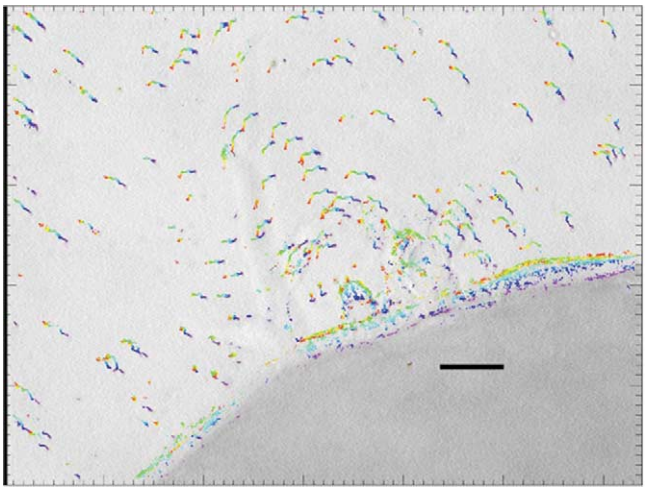

Fig. 6. Time-lapse multiparticle tracking (Day 2). Note a single invasive branch emerging from the darkened MTS. Beads in the bulk gel, not near the invasive cell, show 3–5 μm displacement radially outward. The displacements of beads near the invasive cell, however, show a significant component radially inward, as much as 2 μm in some cases, as bead paths arc over the course of this acquisition (bar = 10 μm; original magnification: ×40; time-lapse duration: 224 min).

continuum elastic medium [25]. If we now treat the traction-induced bead displacements as the result of a point force, applied at the invasive cell tip in a direction determined by averaging displacement vectors, we can estimate the magnitude of this force using the equation of equilibrium for a three-dimensional elastic solid. A displacement **u** will have the following form:

$$\vec{u} = \frac{1+\nu}{8\pi E(1-\nu)} \frac{(3-4\nu)\vec{F} + \vec{n}(\vec{n}\cdot\vec{F})}{r}, \tag{4}$$

where $r = (x^2 + z^2)^{1/2}$ is the distance from the origin where the force is applied, E is the elastic modulus, and ν is Poisson's ratio [26]. For a true point force, Eq. (4) should be valid at all locations where r is large compared to the dimension of the region where the force is applied—in this case, at distances more than a few microns from the invasive tip. If we choose coordinate axes such that $\mathbf{F} = F\mathbf{z}$, the orthogonal components of $\mathbf{u} = w\mathbf{z} + v\mathbf{x}$ can be simplified to yield the following:

$$w = \frac{F(1+\nu)}{8\pi E(1-\nu)r}\left(3 - 4\nu + \frac{z^2}{r^2}\right) \tag{5}$$

and

$$v = \frac{F(1+\nu)}{8\pi E(1-\nu)} \frac{xz}{r^3}. \tag{6}$$

Setting ν, Poisson's ratio, to ½ , and thus approximating the matrix as an incompressible medium, the magnitude of the point force F applied over the time-lapse period can be approximated from observed displacements. From w and v components of the four bead tracks (1–4) indicated in Fig. 7, we estimate that, over the 165 min shown in this time lapse, this invading cell tip pulls nearby gel inward with a force in the range 10–100 nN. The forces thus estimated are significantly less than those reported for fibroblasts as measured on elastic substrates, ~2 μN [6,27], but only about 2–10 times less than those measured at the front of a migrating fibroblast [28] and comparable to the force, up to 30 nN, applied at a single focal adhesion by human foreskin and cardiac fibroblasts [29]. By superposing the displacement field resulting from such a point force with the displacement field caused by a distant, pressurized sphere [26], representing the MTS, we can better approximate the displacement field observed in Fig. 7. In spherical coordinates, the radial and angular strains of a hollow, pressurized sphere with internal and external radii R_{MTS} and R are as follows:

$$u_{\mathrm{rr}} = a - \frac{2b}{r'^3} \tag{7}$$

and

$$u_{\theta\theta} = a + \frac{2b}{r'^3} \tag{8}$$

where r' is the distance from the center of the sphere and a and b are constants determined by the following boundary conditions:

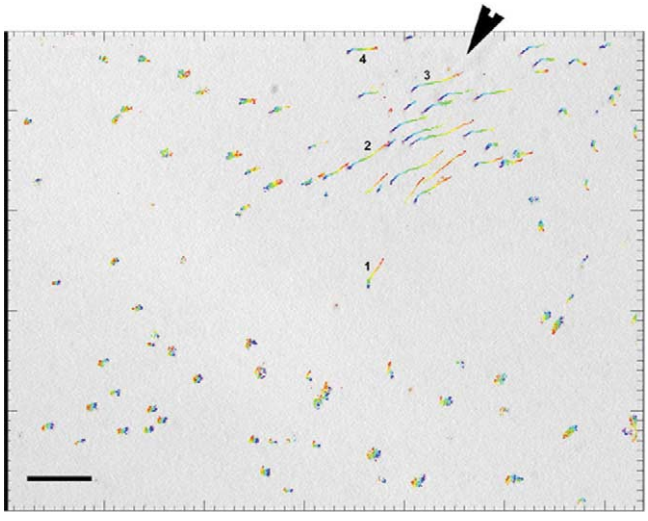

Fig. 7. Time-lapse multiparticle tracking (Day 4). Note the elongated single cell at the tip of the cell branch invading from top right, indicated by the *arrow*. Beads 7–14 μm from the cell tip (tracks 2 and 3) are displaced about 8 μm in toward the tip over this time-lapse observation. A bead (center, right) about 30 μm from the cell tip (track 1) is displaced about 5 μm, whereas beads 46 μm and more distant from the tip show no significant displacement inward. A bead located along a line almost orthogonal to the line of invasion (track 4) shows displacement toward the tip much greater than would be expected to result from a true point force producing the displacements observed for beads located along the line of invasion (tracks 1–3). Beads very far from the invasive tip show a slight displacement outward (bar = 10 μm; original magnification: ×40; time-lapse duration: 165 min).

$$a = \frac{pR_{\mathrm{MTS}}{}^3}{R^3 - R_{\mathrm{MTS}}{}^3}\left(\frac{1-2\nu}{E}\right) \tag{9}$$

and

$$b = \frac{pR_{\mathrm{MTS}}{}^3R^3}{R^3 - R_{\mathrm{MTS}}{}^3}\left(\frac{1+\nu}{2E}\right) \tag{10}$$

for a sphere with internal pressure p and no external pressure. At the time and location shown in Fig. 7, the MTS center is about 260 μm distant from the field of view and the MTS radius is about 130 μm. We take R to be 1 cm, the linear dimension of our sample cube. Although the plexiglass cube, if completely filled with gel, might be expected to provide a confining external pressure, by Day 4 the gel had lost a slight amount of fluid and there was an air-filled gap at the top of the sample cube, which implies that gel expansion should not be constrained by the cube. By superposing these two displacement fields and varying the parameters p and F, we can adjust the resultant field to resemble the observation. An internal pressure of 50 Pa and a point force of 55 nN reproduces bead displacements at many locations to within about 20%. This pressure is much less than the limiting growth pressures [2], which is not surprising because the Fig. 7 time-lapse sequence was taken on Day 4, when volumetric growth was very low. We note, however, that a growing tumor and an invading cell likely consume some of the surrounding medium, so that gel volume is not conserved and the system is not truly Hookean. Furthermore, the way in which proteolytic enzymes may change the gel's elastic properties has not been examined here. Better characterizations of the effects, if any, of enzymatic proteolysis on gel viscoelastic properties and of the rate and spatial distribution of gel consumption by invasive cells will allow refinement of these traction and force estimations, as will measurement of the gel's true Poisson ratio. Moreover, as the cell invades the gel, the point at which the inward force is applied, which we have taken as the origin of our coordinate system above, should move outward with the cell as well. Indeed, this cell-ward force does not seem to be, in fact, a true point force. A more sophisticated treatment, incorporating multiple, moving force origins as well as a model of cell adhesion to and exertion of traction on gel filaments, might significantly improve interpretation of these observations.

On a larger length and longer time scale, observation of the tumor system shows that both spheroid volume and invasion area increase over the observation period. However, these increases are neither monotonic nor synchronized; rather, a marked increase in invasion area (Days 3–4) trails a rapid gain in volume (Days 1–3) and precedes a second rapid volumetric expansion (Days 4–6), as shown in Figs. 2 and 3. A similar pattern has been described previously by Deisboeck et al. [18], and present observations are in agreement with the notion that a *feedback* mechanism may link volumetric growth and invasive expansion. As indicated by time-lapsed observation of bead displacement far from the MTS, the mechanical impact of the microscopic tumor on its environment reaches well beyond a distance, measured from the MTS edge, greater than twice the initial radius of the MTS. Because the clinically relevant, macroscopic situation presents tumor radii of several centimeters [30] and because tumor cells have been found in vivo at a distance greater than 4 cm from the gross tumor [31], a cautious extrapolation of these findings to the clinical situation suggests that the tumor's mechanical impact may be exerted throughout, and perhaps even beyond, the entire ipsilateral brain hemisphere. Interestingly, this notion is already supported by preliminary results from a brain tumor patient, found using specific diffusion-tensor MR imaging, showing tumor-related changes in the diffusion anisotropy of water throughout the brain [32].

Furthermore, we find that marked ECM-gel *invasion* appears to be correlated with tumor cell *traction.* This corresponds well with the findings of Klein et al. [10], who report that two highly aggressive melanoma cell lines efficiently contract 3D collagen type I gels and that their synthesis of $\alpha_2\beta_1$ integrins is upregulated. The upregulation of such cell adhesion receptors is important in this context because integrins mediate also in malignant brain tumor cells both interaction with ECM components and invasiveness [33]. However, the identity of specific mechanism(s) used by tumor cell-generated traction to facilitate directed movement is still unclear. Vernon and Sage [15], for example, propose that traction-mediated alignment of an ECM may produce specific pathways that other cells follow. Davis and Camarillo [34] suggest a similar concept drawn from their studies of endothelial cells, which caused linear distortions of Matrigel; these distortions correspond to the migration pathways of endothelial cell processes. These authors call this phenomenon "matrix guidance pathways" and say it may result from the generation of tension between endothelial cells. Tranquillo [35] presented a similar concept for fibroblasts, proposing that "cells align, exert traction and migrate preferentially in the direction in which surrounding fibrils are aligned." Deisboeck et al. [18] presented a "least resistance, most permission, highest attraction" concept for the emergence of invasive branching patterns: brain tumor cells would follow each other because of increased chemical attraction, enhanced haptotactic permission as well as reduced mechanical resistance within a preformed path. The aforementioned "matrix guidance" would thus be in accordance with this concept as it also facilitates at least the haptotactic element. Our time-lapse observations indicate that the traction-induced tension associated with invasion is highly localized at the tips of invasive branches and not alongside established invasive branches closer to the MTS. The fairly constant average thermal MSD of beads within the area near such invasive cell tips may argue for a relatively minor role of proteolytic enzymes in the tip area, because substantial matrix degradation would be expected to result in an increase in ther-

mally driven bead fluctuations. However, because the parental cell line (U87MG) has been shown to secrete MMP-2, which degrades collagen IV, a component of GFR–Matrigel, and because the release of MMP-2 has been linked to collagen contraction by endothelial cells [13–15], the possibility that proteolytic enzymes may contribute to tumor invasion also in the present study cannot be eliminated. This is further supported by the findings of Vaithilingam et al. [36], who report an (primarily extracellular) increase of general proteolytic activity in C6 astrocytoma spheroids with increasing spheroid diameter.

The 3D assay system used in the current study does have potential shortcomings. For example, the presence of some tissue culture medium around the spheroid when the MTS is implanted cannot be avoided. The early inward gel movement depicted in Fig. 4 probably results from the rapid metabolism of traces of incubation medium by highly proliferative MTS surface cells. Generally, a higher incubation medium concentration might produce an immediate environment that is more favorable for volumetric tumor growth and hence result in the first marked increase of MTS volume (I) in Fig. 2. A loss of fluid from the gel toward the end of the observation period is another concern and might indicate a rather serious limitation of the assay, because the loss of fluid and the resulting increased rigidity of the gel may render forward cell movement more difficult. To address this issue, it is helpful to look carefully at the invasive behavior, depicted in Fig. 3. The invasion area clearly still continues to increase toward the end of the observation period, which suggests a relatively minor influence of drying on cell motility.

In summary, we have demonstrated that an expanding, microscopic tumor system exerts significant mechanical forces upon its environment, in this case a particular extracellular matrix gel composition placed inside a novel plexiglass cube. More specifically (1) the multicellular brain tumor spheroid system exerts both compressive pressure *and* tension on its microenvironment; (2) these mechanical forces can be linked to the tumor's proliferative and invasive growth dynamics, which seem to induce each other; (3) spatially, the mechanical impact of the volumetrically growing tumor propagates to at least twice its initial radius; (4) the growing MTS exerts this outward pressure, but inward traction is generated by invasive tips only; and (5) furthermore, this cell traction does not relax while volumetric growth of the MTS ceases. Also, the invasive tip maintains this tension for 5 consecutive days during which the overall invasive area increases substantially. Cell-imposed traction and tumor invasion therefore seem related.

Acknowledgments

This work was supported in part by Grant CA69246 from the National Institutes of Health and by Grant DMR9971432 from the National Science Foundation. The authors thank Drs. Leonard M. Sander (Department of Physics, University of Michigan); Daniel Fisher (Department of Physics, Harvard University); Michael E. Berens (Neuro-Oncology Laboratory, Barrow Neurological Institute); Andrea Del Vecchio, Xi Chen, and John Hutchinson (all, Division of Engineering and Applied Sciences, Harvard University); Andreas Bausch (Technical University, Muenchen, Germany); and Peter Friedl (University of Wuerzburg, Germany) for inspiring discussions as well as Drs. Maria Kilfoil and You-Yeon Won (both, Division of Engineering and Applied Sciences, Harvard University) for assistance with the rheometer. D.A-A. gratefully acknowledges funding by the Kennedy Memorial Trust.

References

[1] 2002–2003, CBTRUS, Central Brain Tumor Registry of the United States, Statistical Report, 1995–1999 (years data collected).
[2] G. Helmlinger, P.A. Netti, H.C. Lichtenbeld, R.J. Melder, R.K. Jain, Solid stress inhibits the growth of multicellular tumor spheroids, Nat. Biotechnol. 15 (1997) 778 –783.
[3] P. Delvoye, P. Wiliquet, J.-L. Leveque, B.V. Nusgens, C.M. Lapiere, Measurement of mechanical forces generated by skin fibroblasts embedded in a three-dimensional collagen gel, J. Invest. Dermatol. 97 (1991) 898–902.
[4] A.K. Harris, P. Wild, D. Stopak, Silicon rubber substrata: a new wrinkle in the study of cell locomotion, Science 208 (1980) 177–179.
[5] A.K. Harris, D. Stopak, P. Wild, Fibroblast traction as a mechanism for collagen morphogenesis, Nature 290 (1981) 249–251.
[6] M. Dembo, Y.-L. Wang, Stresses at the cell-to-substrate interface during locomotion of fibroblasts, Biophys. J. 76 (1999) 2307–2316.
[7] G. Jenkins, K.L. Redwood, L. Meadows, M.R. Green, Effect of gel re-organization and tensional forces on $\alpha 2\beta 1$integrin levels in dermal fibroblasts, Eur. J. Biochem. 263 (1999) 93–103.
[8] R.B. Vernon, J.C. Angello, M.L. Iruela-Arispe, T.F. Lane, E.H. Sage, Reorganization of basement membrane matrices by cellular traction promotes the formation of cellular networks in vitro, Lab. Invest. 66 (1992) 536–547.
[9] S. Guido, R.T. Tranquillo, A methodology for the systematic and quantitative study of cell contact guidance in oriented collagen gels: correlation of fibroblast orientation and gel birefringence, J. Cell Sci. 105 (1993) 317–331.
[10] C.E. Klein, D. Dressel, T. Steinmayer, C. Mauch, B. Eckes, T. Krieg, R.B. Bankert, L. Weber, Integrin $\alpha 2\beta 1$ is upregulated in fibroblasts and highly aggressive melanoma cells in three-dimensional collagen lattices and mediates the reorganization of collagen I fibrils, J. Cell Biol. 115 (1991) 1427–1436.
[11] G. Apodaca, J.T. Rutka, K. Bouhana, M.E. Berens, J.R. Giblin, M.L. Rosenblum, J.H. McKerrow, M.J. Banda, Expression of metalloproteinases and metalloproteinase inhibitors by fetal astrocytes and glioma cells, Cancer Res. 50 (1990) 2322–2329.
[12] A. Nakano, E. Tani, K. Miyazaki, Y. Yamamoto, J.I. Furuyama, Matrix metalloproteinases and tissue inhibitors of metalloproteinases in human gliomas, J. Neurosurg. 83 (1995) 298–307.
[13] J.H. Uhm, N.P. Dooley, J.G. Villemure, V.W. Yong, Glioma invasion in vitro: regulation by matrix metalloprotease-2 and protein kinase C, Clin. Exp. Metastasis 14 (1996) 421–433.
[14] S.K. Chintala, J.C. Tonn, J.S. Rao, Matrix metalloproteinases and their biological function in human gliomas, Int. J. Dev. Neurosciences 17 (1999) 495–502.
[15] R.B. Vernon, E.H. Sage, Contraction of fibrillar type I collagen by endothelial cells: a study in vitro, J. Cell Biochem. 60 (1996) 185–197.

[16] R.M. Sutherland, Cell and environment interactions in tumor microregions: the multicell spheroid model, Science 240 (1988) 177–184.
[17] R. Nishikawa, X.D. Ji, R.C. Harmon, C.S. Lazar, G.N. Gill, W.K. Cavenee, H.J. Huang, A mutant epidermal growth factor receptor common in human glioma confers enhanced tumorigenicity, Cancer Res. 91 (1994) 7727–7731.
[18] T.S. Deisboeck, M.E. Berens, A.R. Kansal, S. Torquato, A.O. Stemmer-Rachamimov, E.A. Chiocca, Pattern of self-organization in tumour systems: complex growth dynamics in a novel brain tumour spheroid model, Cell Proliferation 34 (2001) 115–134.
[19] J.M. Harris, S. Zalipsky, Poly(ethylene glycol): Chemistry and Biological Applications 1997, American Chemical Society, Washington, DC.
[20] M.T. Valentine, Z. Perlman, M.L. Gardel, J. Shin, P.T. Matsudaira, L. Mahadevan, T. Mitchison, D.A. Weitz, Effect of surface chemistry on microrheology experiments: comparison of BSA-blocks, PEG-coated, and carboxylated beads, in preparation.
[21] J.C. Crocker, D.G. Grier, Methods of digital video microscopy for colloidal studies, J. Colloid Interface Sci. 179 (1996) 298–310.
[22] T.G. Mason, D.A. Weitz, Optical measurements of frequency-dependent linear viscoelastic moduli of complex fluids, Phys. Rev. Lett. 74 (1995) 1250–1253.
[23] M.T. Valentine, P.D. Kaplan, D. Thota, J.C. Crocker, T. Gisler, R.K. Prud'homme, M. Beck, D.A. Weitz, Investigating the microenvironments of inhomogeneous soft materials with multiple particle tracking, Phys. Rev. E 64 (2001) 061506.
[24] H.K. Kleinman, M.L. McGarvey, J.R. Hassell, V.L. Star, F.B. Cannon, G.W. Laurie, G.R. Martin, Basement membrane complexes with biological activity, Biochemistry 25 (1986) 312–318.
[25] S.P. Timoshenko, J.N. Goodier, Theory of Elasticity. 3rd ed, 1987, McGraw-Hill, New York.
[26] L.D. Landau, E.M. Lifshitz, Theory of Elasticity. 3rd ed, 1986, Pergamon Books Ltd., New York.
[27] L.K. Wrobel, T.R. Fray, J.E. Molloy, J.J. Adams, M.P. Armitage, J.C. Sparrow, Contractility of single human dermal myofibroblasts and fibroblasts, Cell Motil. Cytoskeleton 52 (2002) 82–90.
[28] C.G. Galbraith, M.P. Sheetz, A micromachined device provides a new bend on fibroblast traction forces, Proc. Natl. Acad. Sci. USA 94 (1997) 9114–9118.
[29] N.Q. Balaban, U.S. Schwarz, D. Riveline, P. Goichberg, G. Tzur, I. Sabanay, D. Mahalu, S. Safran, A. Bershadsky, L. Addadi, B. Geiger, Force and focal adhesion assembly: a close relationship studied using elastic micropatterned substrates, Nat. Cell Biol. 3 (2001) 466–472.
[30] A.R. Kansal, S. Torquato, G.R. Harsh IV, E.A. Chiocca, T.S. Deisboeck, Simulated brain tumor growth dynamics using a three-dimensional cellular automaton, J. Theor. Biol. 203 (2000) 367–382.
[31] D.L. Silbergeld, M.R. Chicoine, Isolation and characterization of human malignant glioma cells from histologically normal brain, J. Neurosurg. 86 (1997) 525–531.
[32] S. Zhang, D.H. Laidlaw, M.E. Bastin, S. Sinha, T.S. Deisboeck. Computational visualization and analysis of structural heterogeneity in a diffusion tensor MRI-data set from a brain tumor patient, submitted.
[33] W. Paulus, J.C. Tonn, Basement membrane invasion of glioma cells is mediated by integrin receptors, J. Neurosurg. 80 (1994) 515–519.
[34] G.E. Davis, C.W. Camarillo, Regulation of endothelial cell morphogenesis by integrins, mechanical forces, and matrix guidance pathways, Exp. Cell Res. 216 (1995) 113–123.
[35] R.T. Tranquillo, Self-organization of tissue equivalents: the nature and role of contact guidance, Biochem. Soc. Symp. 65 (1999) 27–42.
[36] I.S. Vaithilingam, E.C. Stroude, W. McDonald, R.F. Del Maestro, General protease and collagenase (IV) activity in C6 astrocytoma cells, C6 spheroids and implanted C6 spheroids, J. Neuro-Onc. 10 (1991) 203–212.